Acta Geotechnica (2016) 11:763–774
DOI 10.1007/s11440-015-0412-x

RESEARCH PAPER

An experimental database for the development, calibration and verification of constitutive models for sand with focus to cyclic loading: part II—tests with strain cycles and combined loading

Torsten Wichtmann[1] · **Theodoros Triantafyllidis**[1]

Received: 12 November 2014 / Accepted: 29 July 2015 / Published online: 29 August 2015

Abstract For numerical studies of geotechnical structures under earthquake loading, aiming to examine a possible failure due to liquefaction, using a sophisticated constitutive model for the soil is indispensable. Such model must adequately describe the material response to a cyclic loading under constant volume (undrained) conditions, amongst others the relaxation of effective stress (pore pressure accumulation) or the effective stress loops repeatedly passed through after a sufficiently large number of cycles (cyclic mobility, stress attractors). The soil behaviour under undrained cyclic loading is manifold, depending on the initial conditions (e.g. density, fabric, effective mean pressure, stress ratio) and the load characteristics (e.g. amplitude of the cycles, application of stress or strain cycles). In order to develop, calibrate and verify a constitutive model with focus to undrained cyclic loading, the data from high-quality laboratory tests comprising a variety of initial conditions and load characteristics are necessary. It is the purpose of these two companion papers to provide such database collected for a fine sand. Part II concentrates on the undrained triaxial tests with strain cycles, where a large range of strain amplitudes has been studied. Furthermore, oedometric and isotropic compression tests as well as drained triaxial tests with un- and reloading cycles are discussed. A combined monotonic and cyclic loading has been also studied in undrained triaxial tests. All test data presented herein will be available from the homepage of the first author. As an example of the examination of an existing constitutive model, the experimental data are compared to element test simulations using hypoplasticity with intergranular strain.

Keywords Combined monotonic and cyclic loading · Cyclic triaxial tests · Database · Fine sand · Isotropic compression tests · Oedometric compression tests · Strain cycles · Un- and reloading cycles

1 Introduction

In the companion paper [12], the data from purely monotonic or cyclic tests with stress cycles have been presented. This paper documents undrained cyclic triaxial tests performed with strain cycles. A first test series with relatively small strain amplitudes ($4 \times 10^{-4} \leq \varepsilon_1^{\text{ampl}} \leq 8 \times 10^{-4}$) was followed by another one with larger cycles ($5 \times 10^{-3} \leq \varepsilon_1^{\text{ampl}} \leq 10^{-2}$). Furthermore, oedometric, isotropic compression or triaxial tests with a combined monotonic and cyclic loading are presented.

In order to give an example for an examination of the prediction of a constitutive model, some of the laboratory experiments have been recalculated using hypoplasticity with intergranular strain [4, 7] as the constitutive model. The model prediction is compared to the experimental results.

2 Undrained tests with strain cycles

2.1 Small strain amplitudes $\varepsilon_1^{\text{ampl}} \leq 8 \times 10^{-4}$

Typical data from tests with strain cycles of relatively small amplitude applied under undrained conditions are

✉ Torsten Wichtmann
torsten.wichtmann@kit.edu

[1] Institute of Soil Mechanics and Rock Mechanics (IBF), Karlsruhe Institute of Technology (KIT), Karlsruhe, Germany

provided in Fig. 1. All three samples were medium dense. In tests TCUE1 and TCUE2, the samples were anisotropically consolidated at $p_0 = 200\,\text{kPa}$ and $\eta_0 = 0.75$ (triaxial compression), while the initial stress was $p_0 = 200\,\text{kPa}$ and $\eta_0 = -0.50$ (triaxial extension) in test TCUE3. Afterwards, the axial strain was oscillated with an amplitude $\varepsilon_1^{\text{ampl}} = 6 \times 10^{-4}$, i.e. the axial strain accumulation rate was zero in these tests ($\dot{\varepsilon}_1^{\text{acc}} = 0$). Tests TCUE1 and TCUE2 differ from each other with respect to the first cycle. In test TCUE2, a first drained cycle was applied (also with

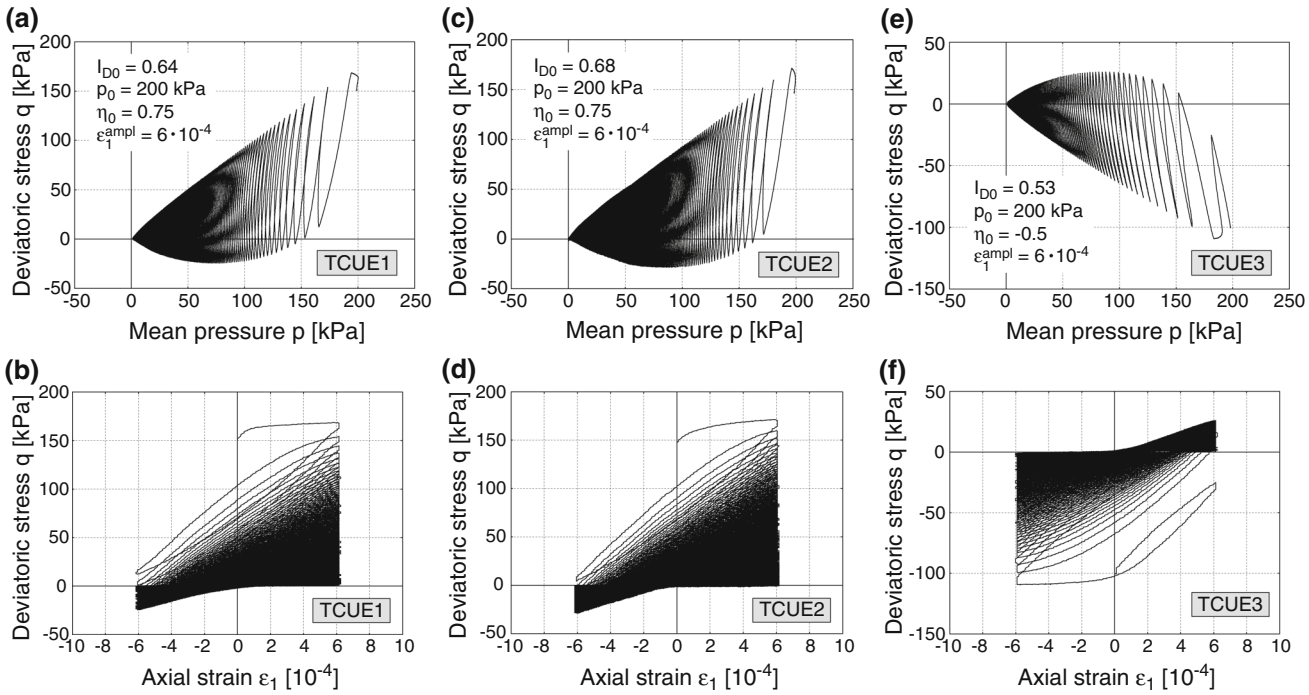

Fig. 1 Effective stress paths and stress–strain relationships in undrained cyclic triaxial tests with anisotropic initial stresses and relatively small strain cycles ($\varepsilon_1^{\text{ampl}} = 6 \times 10^{-4}$) applied without (TCUE1, TCUE3) or with (TCUE2) a first drained cycle

Table 1 Programme of undrained cyclic triaxial tests with strain cycles of relatively small amplitude ($\varepsilon_1^{\text{ampl}} \leq 8 \times 10^{-4}$)

Test	e_{0d} (−)	I_{D0d} (−)	e_0 (−)	I_{D0} (−)	p_0 (kPa)	η_0 (−)	$\varepsilon_1^{\text{ampl}}$ (10^{-4})	1. Drained cycle?
TCUE1	–	–	0.812	0.64	200	0.75	6.0	No
TCUE2	0.789	0.70	0.789	0.70	200	0.75	6.0	Yes
TCUE3	–	–	0.854	0.53	200	−0.5	6.0	No
TCUE4	0.829	0.60	0.829	0.60	200	0.75	4.0	Yes
TCUE5	0.794	0.69	0.793	0.69	200	0.75	8.0	Yes
TCUE6	0.910	0.38	0.910	0.38	200	0.75	6.0	Yes
TCUE7	0.746	0.82	0.745	0.82	200	0.75	6.0	Yes
TCUE8	0.805	0.66	0.805	0.66	200	1.15	6.0	Yes
TCUE9	0.802	0.67	0.801	0.67	200	0	6.0	Yes
TCUE10	0.844	0.56	0.844	0.56	200	−0.50	6.0	Yes
TCUE11	0.836	0.58	0.835	0.58	200	−0.75	6.0	Yes
TCUE12	0.834	0.58	0.833	0.59	50	0.75	6.0	Yes
TCUE13	0.788	0.71	0.788	0.71	100	0.75	6.0	Yes
TCUE14	0.806	0.66	0.806	0.66	300	0.75	6.0	Yes

Void ratios e_0 and relative densities I_{D0} measured at initial stress p_0, η_0 prior to undrained cyclic shearing. e_{0d} and I_{D0d} are the values at p_0 prior to the first drained cycle (if applied)

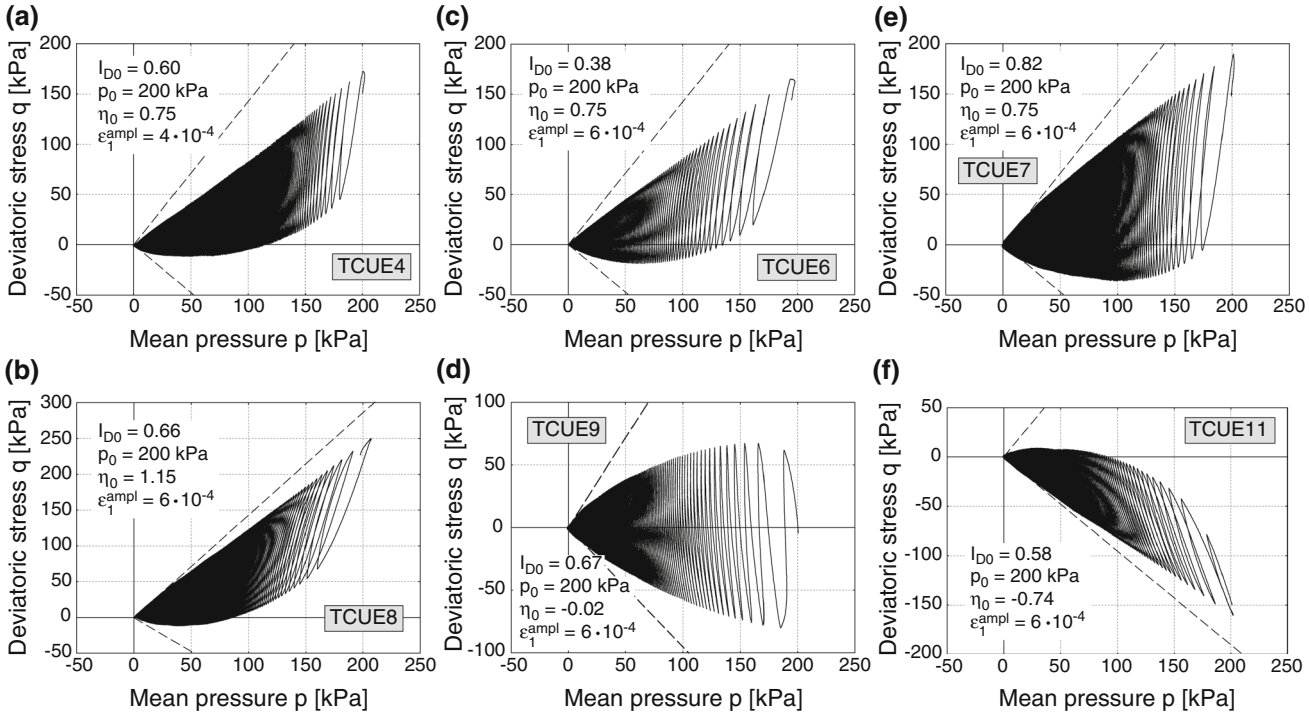

Fig. 2 Effective stress paths in undrained cyclic triaxial tests with relatively small strain cycles ($4 \times 10^{-4} \leq \varepsilon_1^{ampl} \leq 6 \times 10^{-4}$). The initial density I_{D0}, the initial stress ratio η_0 and the strain amplitude ε_1^{ampl} have been varied

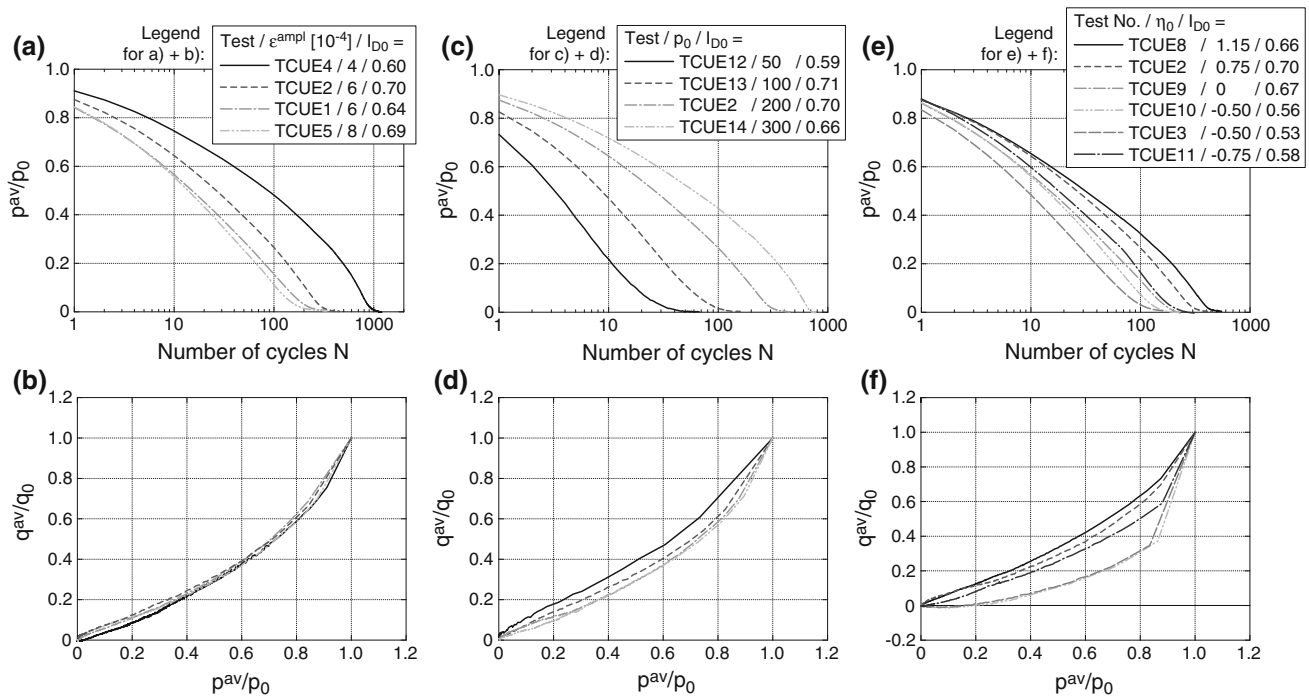

Fig. 3 Relaxation of normalized average mean stress p^{av}/p_0 with increasing number of cycles (*upper row of diagrams*) and effective stress path in q^{av}/q_0–p^{av}/p_0 diagrams (*lower row*). Data from undrained cyclic triaxial tests with relatively small strain cycles $4 \times 10^{-4} \leq \varepsilon_1^{ampl} \leq 8 \times 10^{-4}$

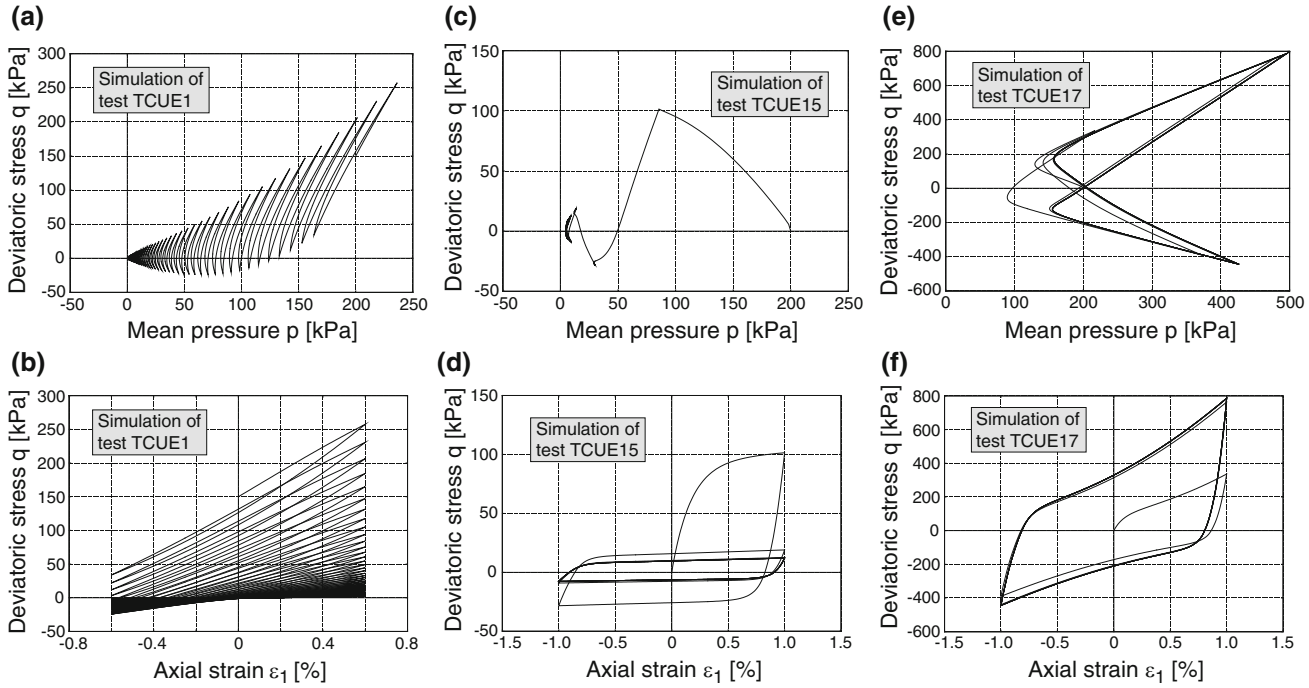

Fig. 4 Simulations with hypoplasticity and intergranular strain of undrained cyclic triaxial tests with strain cycles: **a**, **b** test TCUE1 ($I_{D0} = 0.64$, $p_0 = 200\,\text{kPa}$, $\eta_0 = 0.75$, $\varepsilon_1^{\text{ampl}} = 6 \times 10^{-4}$), **c**, **d** test TCUA15 ($I_{D0} = 0.29$, $p_0 = 200\,\text{kPa}$, $\eta_0 = 0$, $\varepsilon_1^{\text{ampl}} = 1 \times 10^{-2}$), **e**, **f** test TCUA17 ($I_{D0} = 0.94$, $p_0 = 200\,\text{kPa}$, $\eta_0 = 0$, $\varepsilon_1^{\text{ampl}} = 1 \times 10^{-2}$)

Table 2 Programme of undrained cyclic triaxial tests with strain cycles of large amplitude ($\varepsilon_1^{\text{ampl}} \geq 5 \times 10^{-3}$)

Test	e_0 (−)	I_{D0} (−)	p_0 (kPa)	η_0 (−)	$\varepsilon_1^{\text{ampl}}$ (10^{-2})	1. Drained cycle?
TCUE15	0.944	0.29	200	0	1.0	No
TCUE16	0.804	0.66	200	0	1.0	No
TCUE17	0.698	0.94	200	0	1.0	No
TCUE18	0.812	0.64	100	0	1.0	No
TCUE19	0.814	0.64	700	0	1.0	No
TCUE20	0.816	0.63	200	0	0.5	No
TCUE21	0.827	0.60	200	0.75	1.0	No
TCUE22	0.686	0.98	100	0	1.0	No
TCUE23	0.674	1.01	700	0	1.0	No

Void ratios e_0 and relative densities I_{D0} measured at initial stress p_0, η_0 prior to undrained cyclic shearing

$\varepsilon_1^{\text{ampl}} = 6 \times 10^{-4}$), while in test TCUE1, the undrained cyclic loading was started directly after consolidation at p_0, η_0. The strain cycles were applied with a displacement rate of 0.02 mm/min in all tests of this series.

A comparison of the results of tests TCUE1 and TCUE2 in Fig. 1 reveals that the first drained cycle has only a marginal effect on the material response during the subsequent undrained cyclic loading. The strain cycles lead to both an accumulation of pore water pressure (relaxation of p) and a decrease (for $\eta_0 > 0$) or an increase (for $\eta_0 < 0$) in axial effective stress with increasing number of cycles. The effective stress path takes the shape of a fir tree. After a sufficiently large number of cycles, it finally reaches $p = q = 0$, i.e. it ends in a point. Further strain cycles applied in this fully liquefied state are without any further effect on the effective stress.

Several such tests with different strain amplitudes ($4 \times 10^{-4} \leq \varepsilon_1^{\text{ampl}} \leq 8 \times 10^{-4}$), initial stresses ($50\,\text{kPa} \leq p_0 \leq 300\,\text{kPa}$ and $-0.75 \leq \eta_0 \leq 1.15$) and initial relative densities ($0.38 \leq I_{D0} \leq 0.82$) have been performed. The testing programme is summarized in Table 1. Since this test series was originally dedicated to a calibration of the high-cycle accumulation (HCA) model of Niemunis et al. [5] (in particular of Poisson's ratio ν used in the elastic stiffness of the HCA model), most of these tests have been performed with a first drained cycle and the strain amplitudes have been chosen relatively low, i.e. in a typical range for a high cyclic loading. However, the strain amplitudes in these tests are still larger than the threshold strain amplitude below which no accumulation of excess pore pressure occurs (typically $\gamma^{\text{ampl}} \approx 10^{-4}$ for sand [1, 8]), considering $\gamma = 1.5\varepsilon_1$ for the undrained triaxial tests.

Some of the measured effective stress paths are collected in Fig. 2. Independently of the test conditions, the effective stress path finally reaches a state of zero effective

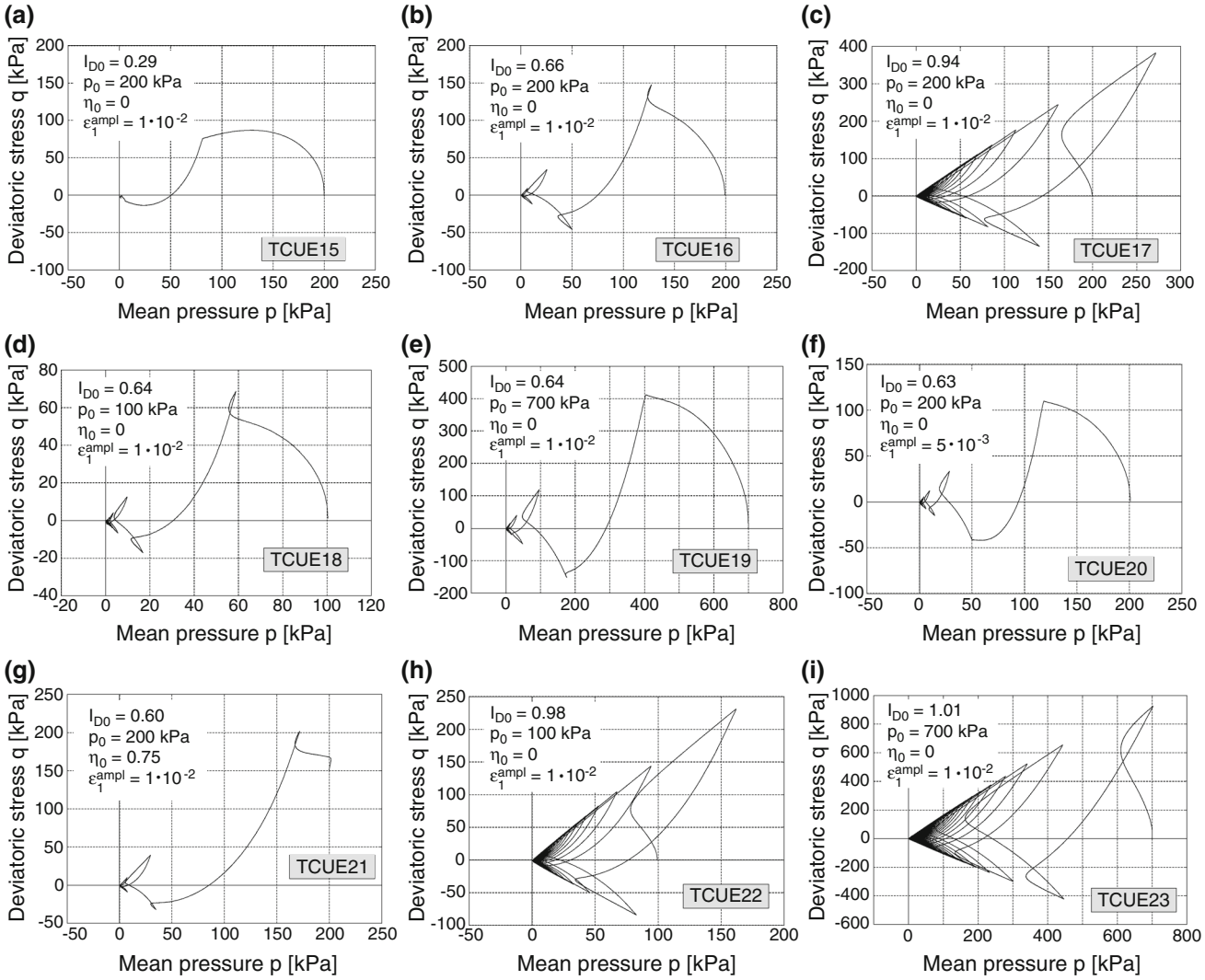

Fig. 5 Effective stress paths measured in undrained cyclic triaxial tests with strain cycles of large amplitude

stress ($p = q = 0$). Of course, the number of cycles necessary to reach this state depends on the amplitude, initial density and initial stress. Similar data as those shown in Figs. 1 and 2 have been documented, e.g. in [2, 3, 6].

The development of normalized average mean stress p^{av}/p_0 with increasing number of cycles is shown in the first row of diagrams in Fig. 3. All curves start from $p^{av}/p_0 = 1$ at $N = 0$. The corresponding average effective stress paths are provided in normalized q^{av}/q_0–p^{av}/p_0 diagrams in the second row of Fig. 3. Stress relaxation occurs faster for larger strain amplitudes ε_1^{ampl} (Fig. 3a), lower initial densities (not shown in Fig. 3), lower initial pressures p_0 (Fig. 3c) and (with the exception of the test at $\eta_0 = -0.75$) lower initial stress ratios η_0 (Fig. 3e). The shape of the normalized average effective stress path is rather independent of strain amplitude (Fig. 3b) and density and only moderately affected by the initial pressure (Fig. 3d). For a given p^{av}/p_0 value, the normalized average deviatoric stress q^{av}/q_0 is larger for higher amounts of the initial stress ratios $|\eta_0|$ (Fig. 3f). For a more detailed analysis of the average effective stress paths, it is referred to [11].

A simulation of test TCUE1 with the hypoplastic model with intergranular strain [4, 7] is presented in Fig. 4a, b. The stress relaxation to $p = q = 0$ is reproduced by the constitutive model. Both the effective stress path and the stress–strain relationship look similar as measured in the test (compare Fig. 1a, b). With the exception of the first two or three cycles, the rate of stress relaxation predicted by the constitutive model is, however, larger than that observed experimentally.

2.2 Large strain amplitudes $5 \times 10^{-3} \leq \varepsilon_1^{ampl} \leq 10^{-2}$

Nine tests with larger strain amplitudes of $\varepsilon_1^{ampl} = 5 \times 10^{-3}$ or $\varepsilon_1^{ampl} = 10^{-2}$ were performed. These strain amplitudes are closer to typical earthquake conditions than those

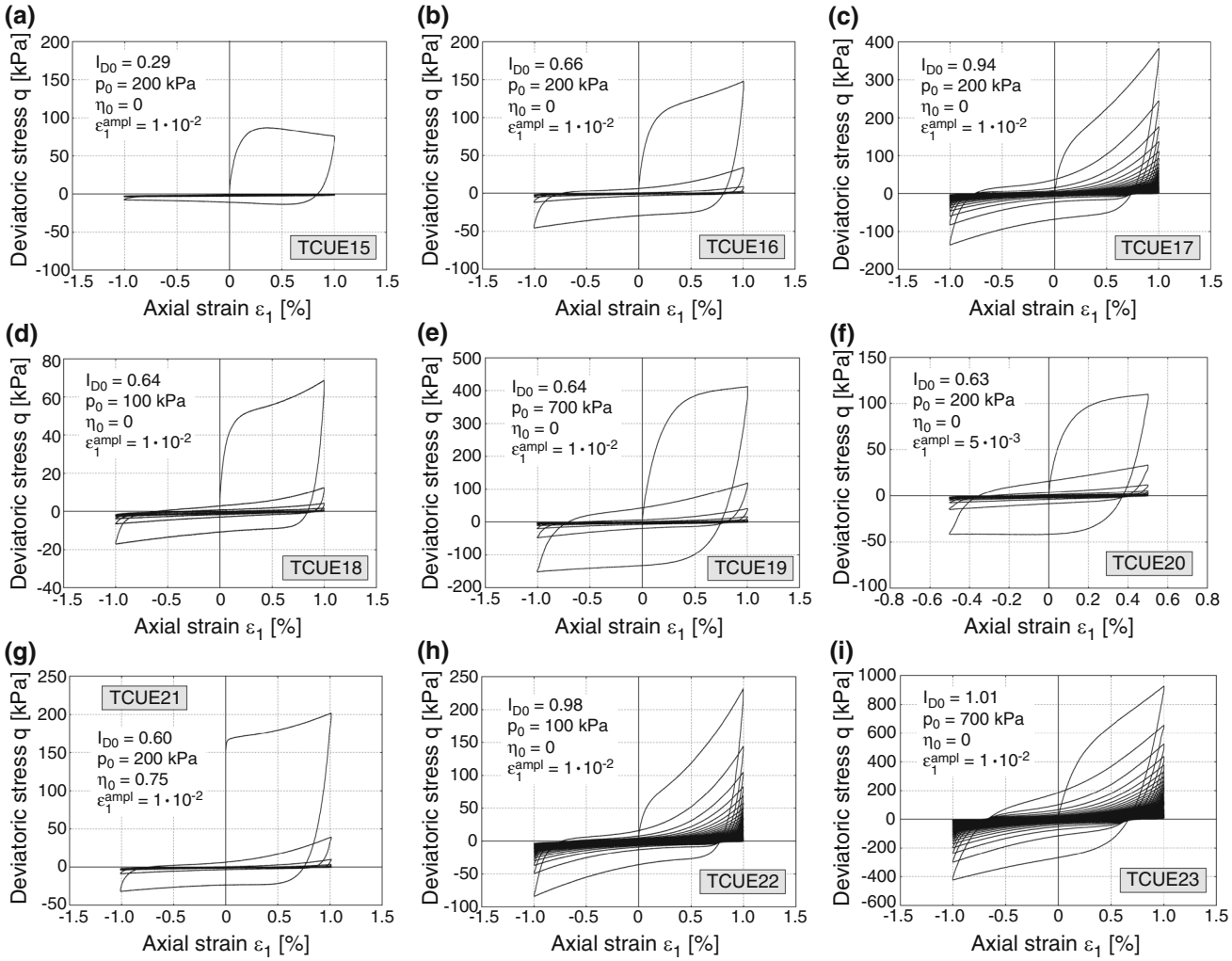

Fig. 6 Stress–strain relationships measured in undrained cyclic triaxial tests with strain cycles of large amplitude

Table 3 Programme of oedometric compression tests with four un- and reloading cycles

Test no.	e_0 (−)	I_{D0} (−)
OEC1	0.998	0.15
OEC2	0.890	0.44
OEC3	0.792	0.70
OEC4	0.756	0.79

Void ratios and relative densities measured at axial stress $\sigma_1 = 0$

applied in the previous test series. The testing programme is given in Table 2. A displacement rate of 0.05 mm/min was used for these tests. The measured effective stress paths are provided in Fig. 5, while the stress–strain relationships are summarized in Fig. 6. The diagrams in the first row of Figs. 5 and 6 belong to tests TCUE15–TCUE17 with different densities ($I_{D0} = 0.29$, 0.66 or 0.94) but identical consolidation stress ($p_0 = 200$ kPa, $\eta_0 = 0$) and strain amplitude ($\varepsilon_1^{ampl} = 10^{-2}$). The loose sample in test TCUE15 liquefied within a single cycle (Fig. 5a), while some more cycles could be applied to the medium dense sample in test TCUE16 until $p = q = 0$ was reached (Fig. 5b). Even in the test TCUE17 on the dense sample, a liquefaction was observed after a sufficiently large number of cycles (Fig. 5c).

In tests TCUE18 and TCUE19, lower ($p_0 = 100$ kPa) or higher ($p_0 = 700$ kPa) initial pressures were tested on medium dense samples (Figs. 5d, e and 6d, e). The initial stress ratio $\eta_0 = 0$ and the strain amplitude $\varepsilon_1^{ampl} = 10^{-2}$ were chosen identical to the tests TCUE15–TCUE17. Test TCUE20 (Figs. 5f and 6f) was performed with a lower strain amplitude ($\varepsilon_1^{ampl} = 5 \times 10^{-3}$) and test TCUE21 (Figs. 5g and 6g) with an anisotropic consolidation ($\eta_0 = 0.75$). Finally, very dense samples were tested at $p_0 = 100$ or 700 kPa, respectively, in the two tests

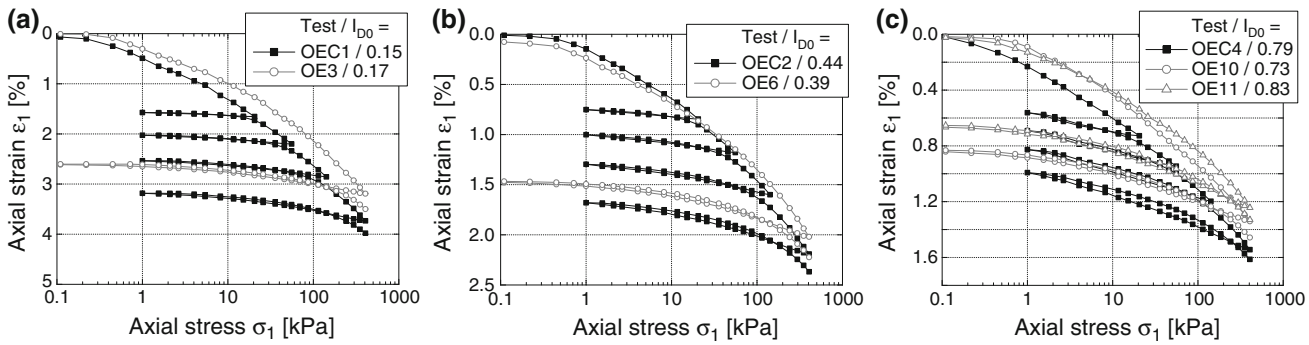

Fig. 7 Axial strain ε_1 versus axial stress σ_1 measured in oedometric compression tests with un- and reloading cycles performed on samples with different initial relative densities

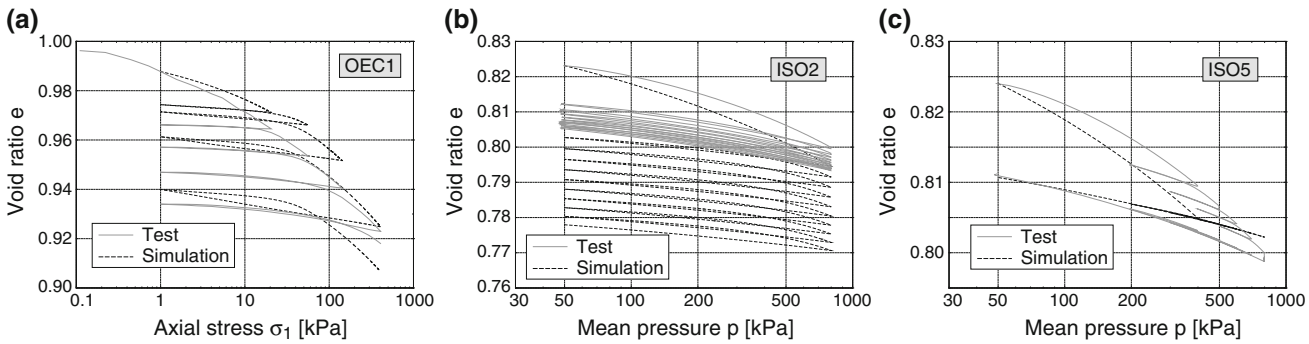

Fig. 8 Simulations of **a** oedometric and **b**, **c** isotropic compression tests with un- and reloading cycles

Table 4 Programme of isotropic compression tests with un- and reloading cycles

Test no.	e_0 (−)	I_{D0} (−)	Cycles	p^{ampl} (kPa)
ISO1	0.974	0.21	Large	750
ISO2	0.823	0.61	Large	750
ISO3	0.690	0.97	Large	750
ISO4	0.963	0.24	Small	200
ISO5	0.824	0.61	Small	200
ISO6	0.680	0.99	Small	200

Void ratios e_0 and relative densities I_{D0} measured prior to isotropic compression at $p_0 = 50$ kPa and $\eta_0 = 0$. p^{ampl} = amplitude of the cycles

TCUE22 and TCUE23 (Figs. 5h, i and 6h, i). For all tested combinations of I_{D0}, p_0, η_0 and $\varepsilon_1^{\text{ampl}}$, a zero effective stress ($p = q = 0$) was reached after a certain number of cycles. This was observed even for the test TCUE23 with an initial density of $I_{D0} = 1.01$. Note that for the calculation of I_{D0} the void ratio e_0 at p_0 is referred to the limit void ratios $e_{\min}$ and $e_{\max}$ determined from standard tests at $p = 0$. The I_{D0} value would be somewhat lower if pressure-dependent limits $e_{\min}(p)$ and $e_{\max}(p)$ had been applied.

Simulations of tests TCUA15 and TCUA17 performed with $\varepsilon_1^{\text{ampl}} = 1 \times 10^{-2}$ on loose or dense fine sand are presented in Fig. 4c–f. In these simulations, an eight-shaped effective stress path is repeatedly passed through after a certain number of cycles. The higher the density, the larger is its distance to the origin of the p–q-plane. A liquefaction as observed in the experiments, independently of density, is not reached in the simulations. Figure 4 reveals that the prediction of hypoplasticity with intergranular strain for undrained tests with large strain cycles is not satisfying, especially when high initial densities are involved.

3 Tests with a combination of monotonic and cyclic loading

3.1 Oedometric compression tests

Four stress-controlled oedometric compression tests were performed on dry samples ($d = 150$ mm, $h = 30$ mm) with different initial relative densities $0.15 \leq I_{D0} \leq 0.79$. The loading to the maximum axial stress of $\sigma_1 = 400$ kPa was interrupted by four un- and reloading cycles each with a minimum stress of $\sigma_1 = 1$ kPa. The testing programme is given in Table 3. The σ_1–ε_1 curves from three of these tests are shown in black colour in the σ_1–ε_1 diagrams in Fig. 7.

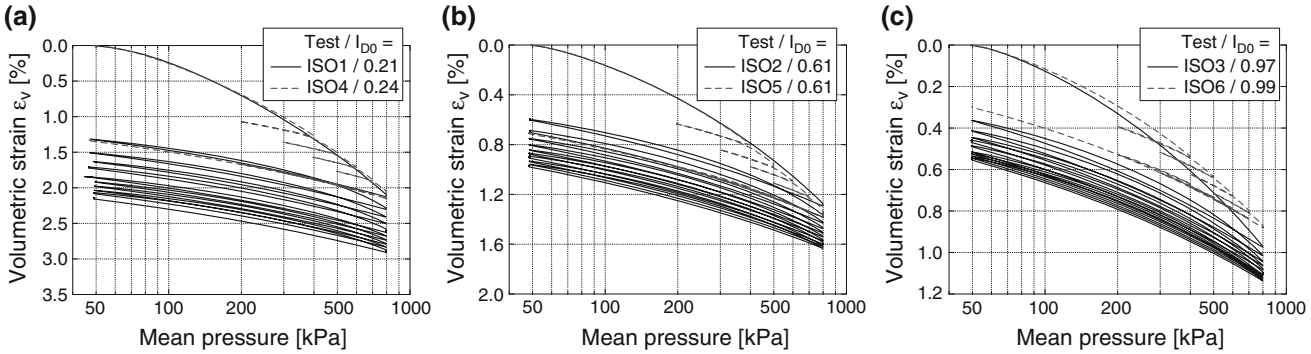

Fig. 9 Volumetric strain ε_v versus effective mean pressure p measured in isotropic compression tests with un- and reloading cycles performed on samples with different initial relative densities

Table 5 Programme of drained triaxial tests with large un- and reloading cycles

Test	e_0 (−)	I_{D0} (−)	p_0 (kPa)	$\Delta\varepsilon_1$ (%)
TMCD1	0.962	0.24	100	2
TMCD2	0.829	0.60	100	2
TMCD3	0.701	0.94	100	2
TMCD4	0.820	0.62	100	6
TMCD5	0.821	0.62	100	12
TMCD6	0.810	0.65	200	2
TMCD7	0.814	0.64	50	2

Void ratios e_0 and relative densities I_{D0} measured at isotropic initial stress p_0 prior to shearing. $\Delta\varepsilon_1$ = strain increment between subsequent un- and reloading cycles

For comparison purpose, the data from tests with similar initial density but only one un- and reloading cycle performed at the end of the test (see Table 1 in [12]) have been added as the grey curves in Fig. 7.

A simulation of test OEC1 with $I_{D0} = 0.15$ is presented in Fig. 8a. The simulation starts at $\sigma_1 = 1$ kPa with intergranular strain fully mobilized in the vertical direction ($h_{11} = -R$). Besides a slightly too large predicted initial stiffness, an "overshooting" of the numerical $e(\sigma_1)$ curve in the first un- and reloading cycle and a "ratcheting", i.e. a too large accumulation of strain in the last two cycles, is obvious in Fig. 8a. The predictions for the tests with higher initial density look very similar to that given in Fig. 8a.

3.2 Drained isotropic compression tests

A drained isotropic compression was tested on six samples with different initial densities ($0.21 \leq I_{D0} \leq 0.99$). In three tests (ISO1–ISO3 in Table 4), ten cycles between $p^{\min} = p_0 = 50$ kPa and $p^{\max} = 800$ kPa were applied. The resulting curves of volumetric strain ε_v versus effective mean pressure p are provided in Fig. 9 (black solid curves). In three other tests, the loading from $p_0 = 50$ kPa to $p = 800$ kPa and back was interrupted by four smaller un- and reloading cycles with $p^{\max} - p^{\min} = 200$ kPa (ISO4–ISO6 in Table 4). The measured data $\varepsilon_v(p)$ from these tests are given as dashed grey curves in Fig. 9.

Simulations of tests ISO2 and ISO5 performed on medium dense samples are presented in Fig. 8b, c. For the test ISO2 with large un- and reloading cycles, the predicted initial stiffness is somewhat too low and the rate of strain accumulation is significantly too large compared to the experimental results (ratcheting, Fig. 8b). Similar to the recalculations of the oedometric tests, the simulation of test ISO5 reveals an overshooting of the $e(p)$ curve (Fig. 8c).

3.3 Drained triaxial tests with large un- and reloading cycles

In seven drained triaxial tests, the monotonic shearing with a displacement rate 0.1 mm/min was interrupted several times by an unloading to $q = 0$ followed by a reloading. The strain increment between the subsequent un- and reloading cycles ($\Delta\varepsilon_1 = 2$, 6 and 12 %) has been varied as well as the initial density of the samples ($0.24 \leq I_{D0} \leq 0.94$) and the effective confining pressure ($\sigma'_3 = p_0 = 50$, 100 and 200 kPa). The testing programme is summarized in Table 5. The q–ε_1- and ε_v–ε_1 diagrams for some of these tests are given in Fig. 10. The data of the tests with a combined monotonic and cyclic loading (black curves in Fig. 10) are compared to the results of purely monotonic tests (grey curves) with similar initial density (Table 3 in [12]). The un- and reloading cycles cause compaction leading to a less pronounced overall dilatancy in the combined tests compared to the purely monotonic loading. The slight "overshooting" of the deviatoric stress during the reloading process may also be attributed to the compaction caused by the cycles, since the density at the end of reloading has increased compared to the state directly before unloading. Furthermore, the peak deviatoric stresses

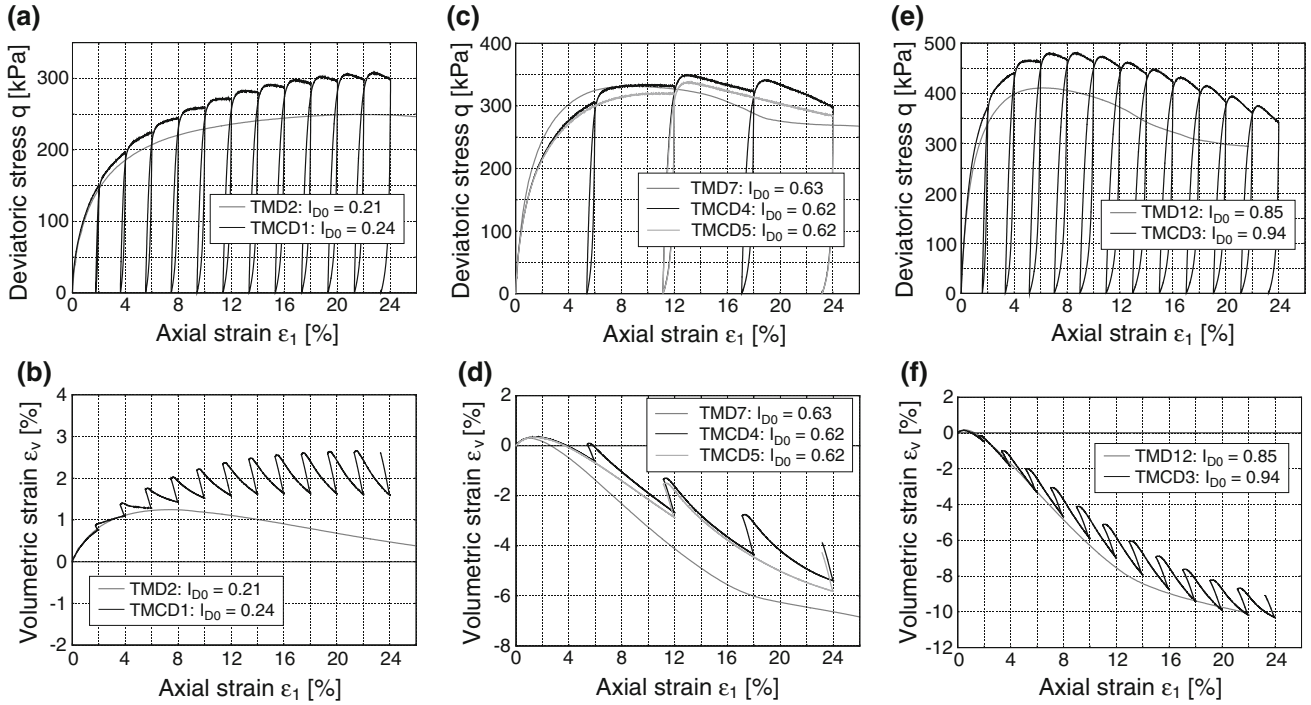

Fig. 10 Stress–strain and dilatancy relationships measured in drained triaxial tests with large un- and reloading cycles

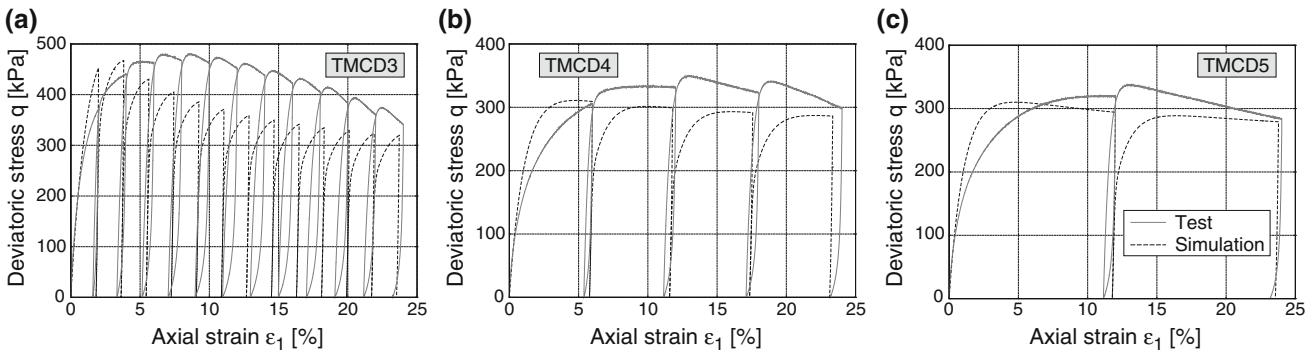

Fig. 11 Simulations of drained triaxial tests with large un- and reloading cycles

are larger in the combined tests. In [9], the data from this test series has been used to calibrate engineering models for the prediction of long-term deformations of offshore wind power plant foundations. Similar results from tests on medium coarse Karlsruhe sand have been presented by Wu [13].

Simulations of three of these tests are shown in Fig. 11. The comparison with the experimental results demonstrates a too stiff prediction of the material response during the first loading prior to the first un- and reloading cycle, while the stiffness decrease during the final stage of the reloading phases is too large. The latter observation agrees with the ratcheting in the simulations of oedometric and isotropic compression tests.

3.4 Undrained triaxial tests with a combination of small strain cycles and monotonic loading

In four tests, strain cycles with an amplitude $\varepsilon_1^{\text{ampl}} = 6 \times 10^{-4}$ were superposed by a monotonic loading performed with rates between $\dot{\varepsilon}_1^{\text{acc}} = 2 \times 10^{-5}$ and $\dot{\varepsilon}_1^{\text{acc}} = 3 \times 10^{-4}$ ($\dot{\varepsilon}_1^{\text{acc}}$ = prescribed monotonic strain per cycle, see testing program in Table 6). A schematic drawing of the test control is given in Fig. 12e. The displacement rate was 0.05 mm/min in all tests of this series. The effective stress paths and stress–strain relationships obtained from the tests with $\dot{\varepsilon}_1^{\text{acc}} = 5 \times 10^{-5}$, 1×10^{-4} and 3×10^{-4} are shown in the p–q-plane in Fig. 12. In the tests with the lower $\dot{\varepsilon}_1^{\text{acc}}$

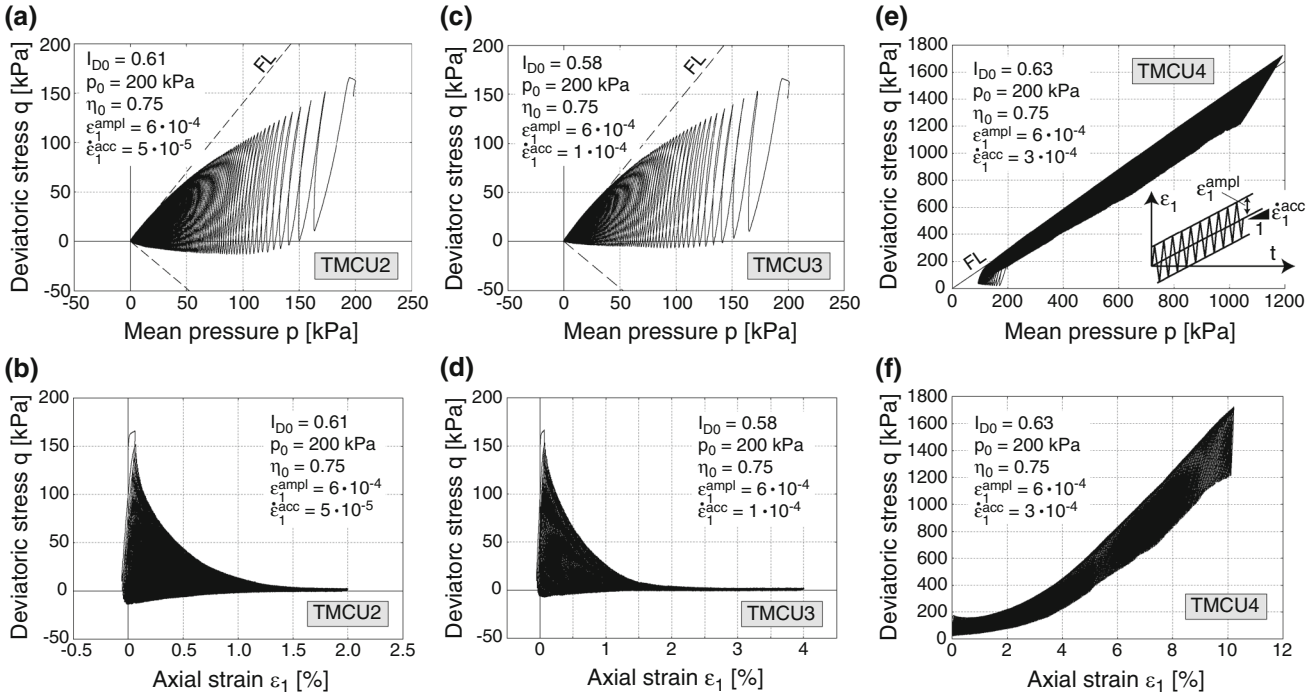

Fig. 12 Effective stress paths and stress–strain relationships measured in undrained cyclic triaxial tests with a combination of monotonic loading (rate $\dot{\varepsilon}_1^{acc}$ per cycle) and small strain cycles (amplitude $\varepsilon_1^{ampl} = 6 \times 10^{-4}$). The three tests have been performed with different values of $\dot{\varepsilon}_1^{acc}$

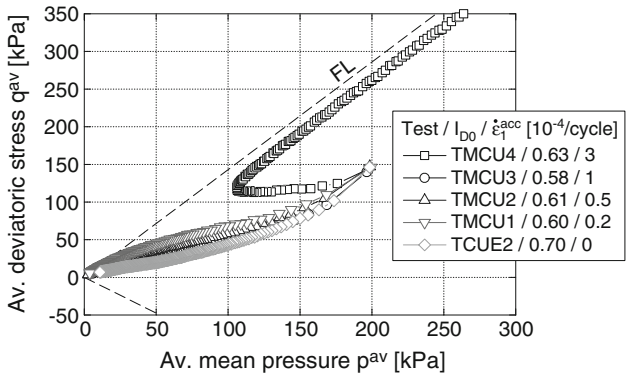

Fig. 13 Average effective stress paths (i.e. p and q values measured at the end of each cycle) in undrained triaxial tests with monotonic compression at a rate $\dot{\varepsilon}_1^{acc}$ superposed by strain cycles with an amplitude $\varepsilon_1^{ampl} = 6 \times 10^{-4}$

values, similar to the tests with $\dot{\varepsilon}_1^{acc} = 0$ (Sect. 2.1), the effective stress path finally reached $p = q = 0$, i.e. the contractive cumulative behaviour due to the strain cycles prevailed over the dilatancy induced by the monotonic shearing (Fig. 12a–d). This is also obvious from the average effective stress paths provided in Fig. 13. The data in Fig. 13 correspond to the p and q values measured at the end of each cycle. In contrast, the dilatancy due to the monotonic loading component prevailed in the case of the largest tested accumulation rate $\dot{\varepsilon}_1^{acc} = 3 \times 10^{-4}$ (Figs. 12e, f and 13). The resulting effective stress path in that test looked similar to that measured in a monotonic test (see, e.g. Fig. 6a,c in [12]), superposed by a cyclic component.

The results of simulations of tests TMCU3 and TMCU4 are provided in Fig. 14a, b. In accordance with the experimental results, the predicted effective stress path ends up at $p = q = 0$ for test TMCU3 with $\dot{\varepsilon}_1^{acc} = 1 \times 10^{-4}$ (Fig. 14a), while the stress path climb along the failure line for TMCU4 with $\dot{\varepsilon}_1^{acc} = 3 \times 10^{-4}$. However, the deviatoric stress q reached in the numerical simulations after approximately 330 cycles is much larger than that observed in the test (Fig. 14b), i.e. the dilatancy predicted by the constitutive model is too large.

3.5 Undrained tests with a combination of stress cycles and monotonic loading

In an undrained test on a medium dense sample ($I_{D0} = 0.67$, $p_0 = 200\,\text{kPa}$, $\eta_0 = 0$, see test TMCU5 in Table 7), the stress cycles ($q^{ampl} = 50\,\text{kPa}$, displacement rate 0.05 mm/min) were stopped shortly before the cyclic mobility phase would have started. The sample was then subjected to an undrained monotonic compression. The measured effective stress path during the monotonic test phase slowly adapts to the failure line known from the purely monotonic undrained tests (Fig. 15a).

The effective stress path and stress–strain relationship provided in Fig. 15b, c were obtained from an undrained

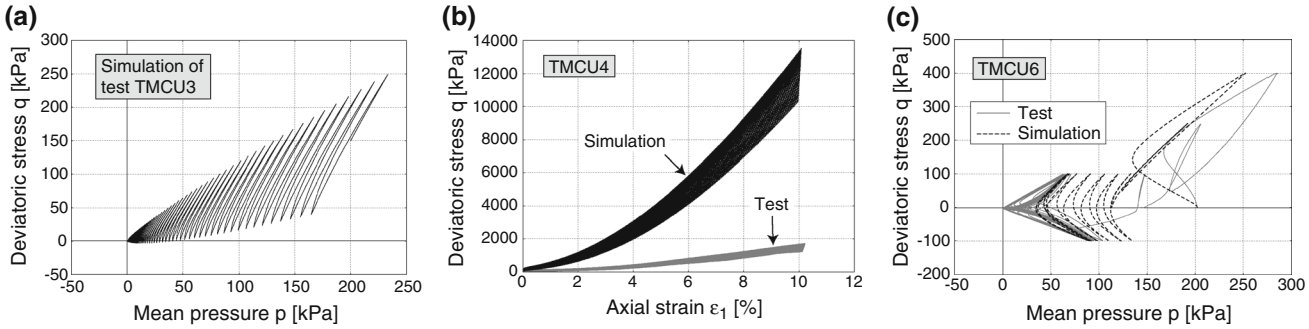

Fig. 14 Simulations of undrained triaxial tests with **a**, **b** monotonic compression at different rates $\dot{\varepsilon}_1^{\text{acc}}$ superposed by strain cycles with an amplitude $\varepsilon_1^{\text{ampl}} = 6 \times 10^{-4}$ and **c** a combination of stress cycles and monotonic loading

Table 6 Programme of undrained triaxial tests with a combination of small strain cycles (amplitude $\varepsilon_1^{\text{ampl}}$) and monotonic loading (rate per cycle $\dot{\varepsilon}_1^{\text{acc}}$)

Test	e_0 (−)	I_{D0} (−)	$\varepsilon_1^{\text{ampl}}$ (10^{-4})	$\dot{\varepsilon}_1^{\text{acc}}$ (10^{-4})
TMCU1	0.827	0.60	6.0	0.2
TMCU2	0.825	0.61	6.0	0.5
TMCU3	0.834	0.58	6.0	1.0
TMCU4	0.816	0.63	6.0	3.0

Void ratios e_0 and relative densities I_{D0} measured at initial stress p_0 prior to undrained cyclic loading

Table 7 Programme of undrained triaxial tests with a combination of monotonic loading and stress cycles

Test	e_0 (−)	I_{D0} (−)	p_0 (kPa)	q^{ampl} (kPa)
TMCU5	0.803	0.67	200	50
TMCU6	0.684	0.98	≈ 140	100

Void ratios e_0 and relative densities I_{D0} measured at initial stress p_0 prior to undrained cyclic loading

test on a very dense sample ($I_{D0} = 0.98$, $p_0 = 200\,\text{kPa}$, $\eta_0 = 0$, displacement rate 0.05 mm/min, see test TMCU6 in Table 7) where the deviatoric stress was first increased to $q = 400\,\text{kPa}$, followed by an unloading to $q = 50\,\text{kPa}$, a reloading to $q = 250\,\text{kPa}$ and another unloading to $q = 0$. Finally, starting from the isotropic stress state, cycles with a stress amplitude $q^{\text{ampl}} = 100\,\text{kPa}$ were applied. Obviously, during the first cycle, a large increase in the pore pressure took place on the extension side ($q < 0$), where the effective stress path follows an elongation of the path measured at $q > 0$ during the preceding unloading phases (Fig. 15b).

The effective stress path obtained from a simulation of test TMCU6 is depicted in Fig. 14c. In particular, the prediction of the material response during the un- and reloading cycle performed between $q^{\min} = 50\,\text{kPa}$ and $q^{\max} = 250\,\text{kPa}$ and that during the first cycle with $q^{\text{ampl}} = 100\,\text{kPa}$ starting from $q = 0$ is unsatisfying, i.e. far away from the experimental curves.

4 Summary and conclusions

The results of cyclic triaxial tests with strain cycles performed on a fine sand have been presented. In all tests, a zero effective stress state ($p = q = 0$) was reached after a sufficiently large number of cycles, irrespective of the applied amplitude (a large range $4 \times 10^{-4} \leq \varepsilon_1^{\text{ampl}} \leq 10^{-2}$ was tested) and the initial values of relative density I_{D0}, mean pressure p_0 or stress ratio $\eta_0 = q_0/p_0$. Even very dense sand ($I_{D0} = 1.01$) finally reached a state of full liquefaction.

Some tests with a combined monotonic and cyclic loading were also performed. Besides oedometric and isotropic compression tests with several un- and reloading cycles, some drained triaxial compression tests were repeatedly interrupted by an unloading to $q = 0$ followed by a reloading. Each un- and reloading cycle causes compaction, and thus a less pronounced overall dilatancy compared to the purely monotonic tests. Furthermore, the maximum deviatoric stresses reached in the tests with the un- and reloading cycles are larger than in the case of a purely monotonic loading.

In undrained tests where small strain cycles ($\varepsilon_1^{\text{ampl}} = 6 \times 10^{-4}$) were superposed by a monotonic loading component, the resulting effective stress path depends on the rate $\dot{\varepsilon}_1^{\text{acc}}$ of monotonic loading (i.e. the prescribed strain per cycle). In case of low rates, the stress relaxation due to the cycles prevails over the dilatancy caused by the undrained monotonic shearing and $p = q = 0$ is finally reached. Larger rates $\dot{\varepsilon}_1^{\text{acc}}$ lead to an effective stress path similar to that observed in the undrained monotonic tests but superposed by some cyclic component.

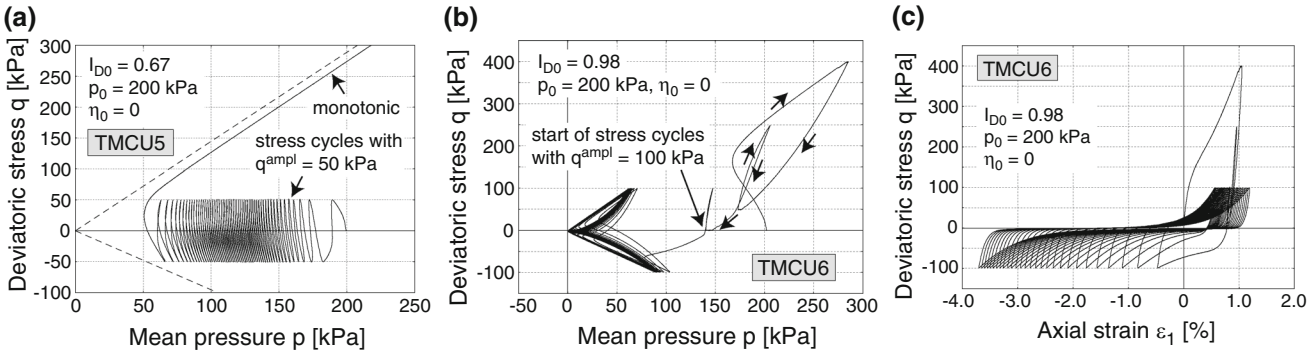

Fig. 15 Effective stress paths or stress–strain relationship measured in undrained cyclic triaxial tests with a combination of stress cycles and monotonic loading

Together with the results from monotonic tests and triaxial tests with stress cycles documented in the companion paper [12], this experimental database may serve for the development, calibration and verification of constitutive models with focus to cyclic loading. All test data presented in this paper will be available from [10].

As an example for the examination of an existing constitutive model based on the presented experimental data, selected tests have been recalculated using hypoplasticity with intergranular strain. The simulations demonstrate that some parts of the material response can be reproduced well (e.g. relaxation to $p \approx q \approx 0$ in tests with small strain cycles $\varepsilon_1^{ampl} \leq 10^{-3}$), while some other experimental observations are not captured sufficiently (e.g. eight-shaped final effective stress loops far away from $p = 0$ in simulations with large strain cycles $\varepsilon_1^{ampl} = 10^{-2}$, ratcheting or over-shooting in the oedometric or isotropic compression tests with un- and reloading cycles). The simulations presented herein and in the companion paper [12] demonstrate the difficulty of reproducing all different kinds of test conditions by a single constitutive model with a limited number of parameters. They highlight the need for further improvements of the existing models or for novel models that deliver a better description of the experimental results. Each reader is encouraged to check his own constitutive model against the database published herein.

Acknowledgments Parts of the presented study have been performed within the framework of the project "Geotechnical robustness and self-healing of foundations of offshore wind power plants" funded by the German Federal Ministry for the Environment, Nature Conservation and Nuclear Safety (BMU, project No. 0327618). Other parts were conducted within the framework of the project "Improvement of an accumulation model for high-cyclic loading" funded by German Research Council (DFG, project No. TR218/18-1 / WI3180/3-1). The authors are grateful to BMU and DFG for the financial support. All tests have been performed by the technicians H. Borowski, P. Gölz and N. Demiral in the IBF soil mechanics laboratory.

References

1. Dobry R, Ladd RS, Yokel FY, Chung RM, Powell D (1982) Prediction of pore pressure buildup and liquefaction of sands during earthquakes by the cyclic strain method. Technical Report 138, U.S. Department of Commerce, National bureau of standards, NBS Building science series
2. Jafarian Y, Towhata I, Baziar MH, Noorzad A, Bahmanpour A (2012) Strain energy based evaluation of liquefaction and residual pore water pressure in sands using cyclic torsional shear experiments. Soil Dyn Earthq Eng 35:13–28
3. Kazama M, Yamaguchi A, Yanagisawa E (2000) Liquefaction resistance from a ductility viewpoint. Soils Found 40(6):47–60
4. Niemunis A, Herle I (1997) Hypoplastic model for cohesionless soils with elastic strain range. Mech Cohes-Frict Mater 2:279–299
5. Niemunis A, Wichtmann T, Triantafyllidis T (2005) A high-cycle accumulation model for sand. Comput Geotech 32(4):245–263
6. Sassa K, Wang G, Fukuoka H, Vankov DA (2005) Shear-displacement-amplitude dependent pore-pressure generation in undrained cyclic loading ring shear tests—an energy approach. J Geotech Geoenviron Eng ASCE 131(6):750–761
7. von Wolffersdorff P-A (1996) A hypoplastic relation for granular materials with a predefined limit state surface. Mech Cohes-Frict Mater 1:251–271
8. Vucetic M (1994) Cyclic threshold shear strains in soils. J Geotech Eng ASCE 120(12):2208–2228
9. Westermann K, Zachert H, Wichtmann T (2014) Vergleich von Ansätzen zur Prognose der Langzeitverformungen von OWEA-Monopilegründungen in Sand. Teil 1: Grundlagen der Ansätze und Parameterkalibration. Bautechnik 91(5):309–323
10. Wichtmann T (2015) www.torsten-wichtmann.de. Homepage
11. Wichtmann T, Niemunis A, Triantafyllidis T (2013) On the "elastic stiffness" in a high-cycle accumulation model—continued investigations. Can Geotech J 50(12):1260–1272
12. Wichtmann T, Triantafyllidis T (2015) An experimental data base for the development, calibration and verification of constitutive models for sand with focus to cyclic loading. Part I: tests with monotonic loading and stress cycles. Acta Geotech. doi:10.1007/s11440-015-0402-z
13. Wu W (1992) Hypoplastizität als mathematisches Modell zum mechanischen Verhalten granularer Stoffe. Veröffentlichungen des Institutes für Boden- und Felsmechanik der Universität Fridericiana in Karlsruhe, Heft Nr. 129